LINEAR STABILITY OF MICROTEARING MODES IN ASDEX

L.Giannone

IPP III/125 December 1987

MAX-PLANCK-INSTITUT FÜR PLASMAPHYSIK

8046 GARCHING BEI MÜNCHEN

LINEAR STABILITY OF MICROTEARING MODES IN ASDEX

L.Giannone

IPP III/125 December 1987

CONTENTS

1. INTRODUCTION

The electron thermal conductivity and diffusion coefficient have been calculated using the neoclassical model of electron transport in a tokamak plasma. However, anomalous particle and energy transport have been experimentally observed [1], with these measurements exceeding theoretical estimates by one and two orders of magnitude, respectively.

The instabilities of an inhomogeneous, magnetised plasma [2] have been used in an attempt to explain this anomalous transport. Drift wave instabilities enhance particle and energy transport across the magnetic field through a correlation between electron density and electric field fluctuations. However, for this type of instability it has been estimated that particle and energy transport are of the same order of magnitude [3].

Electromagnetic instabilitities enhance particle and energy transport through the destruction of magnetic surfaces by the associated stochastic magnetic field fluctuations. Transport across the magnetic field is increased by the coupling of radial transport to the more rapid transport along the magnetic field. Theoretical estimates of transport in the presence of stochastic magnetic field fluctuations are consistent with Alcator scaling in ohmically heated tokamaks.

In particular, microtearing modes [4-11] with poloidal mode numbers in the range 10 to 20 have been shown to be unstable in PLT tokamak [4,5]. In these references model tokamak profiles with equal electron and ion temperatures and $Z = 1$ were assumed.

With the view to providing a theoretical basis for the interpretation of experimental observations of magnetic field fluctuations in ASDEX, the linear stability of microtearing modes are calculated in this report for ASDEX plasmas. Tokamak profiles calculated by the BALDUR code for discharges in the O, L, and H regime are considered.

In section 2, the theory of microtearing modes in a one ion species plasma is reviewed. In section 3, the theory of microtearing modes in a two ion species plasma is developed. The calculation of the parallel electron conductivity from the Fokker-Planck equation is outlined in section 4. The algorithm for the solution of the coupled second order eigenmode equations is presented in section 5. In section 6, a comparison of the resulting eigenvalue with those published in the literature for standard conditions shows that the coding of the algorithm has been successfully performed. The stability of microtearing modes are calculated for ASDEX discharges in the O, L and H regimes. The relevance of these calculations to recent experiments concerned with broadband magnetic fluctuations in tokamaks is discussed in section 7. The conclusions of this report are summarised in section 8, and the references are listed in section 9.

2. MICROTEARING MODES IN A ONE ION SPECIES PLASMA

The tearing instability of a collisional plasma has been recognised [12], and the presence of Mirnov oscillations in a tokamak have been identified with this instability. Since a resistive plasma is not frozen to magnetic field lines, the tearing and reconnection of magnetic field lines is allowed and the plasma relaxs to a state of lower magnetic energy. It has been shown that tearing modes in a tokamak with $m > 4$ are stabilised when the current density profile is sufficiently peaked [13].

An inhomogeneous plasma, with electron density and temperature gradients, requires that the effects of electron and ion drifts be considered. It was found that the tearing mode is destabilised by electron temperature gradients [14]. The drift-tearing or microtearing mode refers to the high m tearing modes driven unstable by electron temperature gradients.

The theory of microtearing modes in a one ion species plasma is carried out in slab geometry, with the plasma embedded in a sheared magnetic field, $\underline{B}$, :

$$\underline{B} = B_o (x/L_s \underline{y} + \underline{z}) \qquad (2.1)$$

The magnetic shear length, L_s, in a tokamak is given by :

$$L_s = R/r_s \; m/n \; q'(r)/q(r) \qquad (2.2)$$

where R is the major radius of the torus, r_s is the radial position of the mode rational surface, m and n are the poloidal and toroidal mode numbers and q(r) is the safety factor. In ASDEX R = 1.67 m and a = 0.40 m. The theoretical model may still be applied to tokamaks by setting $k_y = m/r$ and $k_z = n/R$. In the vicinity of the mode rational surface :

$$k_\parallel = \underline{k}.\underline{B}/|B_o| \approx k_y/L_s \; x + k_z \qquad (2.3)$$
$$\approx k_y/L_s \; x$$

The narrow width of the tearing layer in comparison to the minor radius of the tokamak implies that this simple transformation is justified. However, the

coupling of modes with different m has been neglected [11] and $k_z = 0$ has been chosen. Both of these assumptions are not well justified in toroidal geometry [5].

In a one ion species plasma the plasma beta, β, and the electron beta, β_e, are defined by :

$$\beta = \frac{n_e (T_e + T_i)}{B_o^2/(2\mu_o)} \qquad (2.4)$$

$$\beta_e = \frac{n_e T_e}{B_o^2/(2\mu_o)}$$

where n_e is the electron density

T_e is the electron temperature in energy units

T_i is the ion temperature in energy units

and B_o is the magnitude of the steady magnetic field.

The MKS system of units is adopted in this report.

When $\beta << 1$, the coupling to compressional waves may be neglected and only magnetic field perturbations perpendicular to the magnetic field need be considered. The electric and magnetic field perturbations may then be expressed in terms of the parallel vector potential, $A_{||}$, and the scalar potential, φ :

$$\underline{b} = \nabla \times \underline{A}_{||}$$

$$\underline{E} = -\nabla\varphi - \delta\underline{A}_{||}/\delta t \qquad (2.5)$$

Assuming perturbations of the form :

$$A_{||} = A_{||}(x) \exp \{ i(-\omega t + k_y y + k_{||} z) \}$$

and $$\varphi = \varphi(x) \exp \{ i(-\omega t + k_y y + k_{||} z) \} \qquad (2.6)$$

so that $$E_{||} = i (\omega A_{||} - k_{||}\varphi)$$

then from the component of Ampere's law parallel to the magnetic field [5,11] :

$$(\delta^2/\delta x^2 - k_y^2) A_{||} = - \mu_o j_{||}$$

$$= - i \mu_o \sigma_{||e} (\omega A_{||} - k_{||}\varphi) \qquad (2.7)$$

The contribution to the perturbed current by the ions may be neglected for the modes being considered. The electron parallel conductivity, $\sigma_{\parallel e}$, will be considered in further detail in a later section. Away from the mode rational surface, the perturbed current, $j_{\parallel}$, rapidly approaches zero [11]. In slab geometry, $A_{\parallel}$ decays as $\exp(-k_y x)$. In cylindrical geometry, $A_{\parallel}$ decays as r^{-m}.

Equating the charge density perturbations arising from perturbations in the electron and ion density (the quasi-neutrality condition), gives the relationship governing the fluctuations in φ. The perturbed electron charge density, Q_e, is given by [10] :

$$Q_e = n_{e1}\, e = \frac{-\, k_{\parallel}\sigma_{\parallel e} E_{\parallel}}{\omega} + \frac{n_e e^2}{T_e}\frac{\omega_{*e}}{\omega}\varphi \qquad (2.8)$$

where $\omega_{*e} = k_y T_e/(eBL_n)$ and $L_n = n_e/(\delta n_e/\delta x)$.

The ion density perturbation, n_{i1}, in Fourier space is found by considering the collisionless Vlasov equation [8,11] and is given by :

$$n_{i1}(k) = \frac{-\,(Ze)\, n_i}{\sqrt{2\pi}\, T_i}\left(1 - (\omega + \omega_{*i})/\omega\, F_o(k)\right)\varphi(k) \qquad (2.9)$$

where $\varphi(x) = 1/\sqrt{(2\pi)}\int dk\, \varphi(k)\, e^{ikx}$

$$F_o(k) = I_o(h)\exp(-h)$$

$$h = (k^2 + k_y^2)\,\rho_i^2/2$$

$$\omega_{*i} = k_y T_i/(ZeBL_n)$$

$$\rho_i^2 = (v_i/\omega_{ci})^2 = 2T_i M_i/(eBZ)^2$$

The approximation that $k\rho_i << 1$ is then made. It has been shown that this approximation is not justified in all cases [8]. However, a comparison of results shows that the calculated stability of the mode is only slightly overestimated when using this approximation. The form of the problem is a pair of coupled second order differential equations when this approximation is used,

rather than a second order differential equation and an integral equation. The algorithm for the solution of the coupled pair of second order equations is more straightforward.

Retaining first order terms in the Taylor expansion of $F_o(k)$ leads to the following expression :

$$F_o(k) = (I_o(b) - k^2\rho_i^2/2 \, (I_o(b) - I_1(b))) \exp(-b) \qquad (2.10)$$

with $b = k_y^2\rho_i^2/2$ and I_o, I_1 are the modified Bessel functions [15]. Noting that $I_o'(b) = I_1(b)$ and letting $\Gamma_o(b) = I_o(b)\exp(-b)$ then :

$$F_o(k) = \Gamma_o(b) - k^2\rho_i^2/2 \; |\Gamma_o'(b)| \qquad (2.11)$$

The perturbed ion charge density, Q_i, may be found by Fourier transforming :

$$Q_i = (Ze)\, n_{i1}(x) \qquad (2.12)$$

$$= \frac{-(Ze)^2 n_i}{T_i} [1 - \Gamma_o(b)(\omega+\omega_{*i})/\omega - \rho_i^2/2\,|\Gamma_o'(b)|(\omega+\omega_{*i})/\omega \; \delta^2/\delta x^2] \varphi(x)$$

Assuming $T_e = T_i$ and $Z = 1$, so that $n_i = n_e$, $\omega_{*i} = \omega_{*e}$, and $n_i e^2/T_i = (c^2/v_A^2)(2/\rho_i^2)$, where $v_A^2 = B^2/(\mu_o M_i n_i)$, and letting $\rho_*^2 = \rho_i^2/2$ then :

$$Q_i = - \varepsilon_o(c^2/v_A^2)/(\omega\rho_*^2)$$

$$x \; (\omega - \Gamma_o(b) \, (\omega+\omega_{*i}) - \rho_*^2|\Gamma_o'(b)| \, (\omega+\omega_{*i}) \, \delta^2/\delta x^2 \,) \, \varphi$$

$$Q_e = - ik_\parallel\sigma_{\parallel e}(\omega A_\parallel - k_\parallel\varphi)/\omega + \varepsilon_o(c^2/v_A^2)/\rho_*^2 \, (\omega_{*i}/\omega) \, \varphi \qquad (2.13)$$

Applying the quasi-neutrality condition ($Q_i = Q_e$) yields :

$$c^2/v_A^2 \, (\omega+\omega_{*i}) \, (\, |\Gamma_o'(b)| \, \delta^2/\delta x^2 - (\, 1 - \Gamma_o(b))/\rho_*^2 \,) \, \varphi$$

$$= -ik_\parallel\sigma_{\parallel e}(\omega A_\parallel - k_\parallel\varphi)/\varepsilon_o \qquad (2.14)$$

which is of the same form as equation 3 of reference 5, with the difference due to different definitions of ρ_i. Introducing the following substitutions :

$$\phi = \varphi/v_A$$

$$W = \omega/\omega_{*e}$$

$$C = i\mu_o \, \omega_{*e} \, \rho_i^2 \, \sigma_{\parallel e} \qquad (2.15)$$

$$K = k_\parallel v_A/\omega_{*e} = 2\,(L_n/L_s)\,\sqrt{(2/\beta)}\,X$$

$$X = x/\rho_*$$

enables equations (2.3) and (2.4) to be expressed in the form :

$$\delta^2 A_{\parallel}/\delta X^2 = (k_y^2 \rho_i^2 - CW) A_{\parallel} + (CK) \phi$$

$$\delta^2 \phi/\delta X^2 = \frac{(-CKW) A_{\parallel} + (CK^2 + 2(1 - \Gamma_o)(W + 1)) \phi}{(W + 1) |\Gamma_o'|} \qquad (2.16)$$

In this form the coupled second order differential equation may be solved numerically by the invariant imbedding method [16].

The boundary conditions to be satisfied at the origin are :

$$A_{\parallel}'(0) = \phi(0) = 0 \qquad \text{for the microtearing mode}$$

$$A_{\parallel}(0) = \phi'(0) = 0 \qquad \text{for the drift wave mode} \qquad (2.17)$$

The solution with even parity in $A_{\parallel}$ and odd parity in ϕ is the microtearing mode. For this mode the coupled second order differential equations are invariant under the transformation :

$$X \rightarrow -X$$

$$\phi(X) \rightarrow -\phi(-X)$$

$$A_{\parallel}(X) \rightarrow A_{\parallel}(-X) \qquad (2.18)$$

since the matrix coefficients contain a term in K, and this term has odd parity.

The boundary conditions at $X = \infty$ are given by :

$$\phi(\infty) = 0$$

$$A_{\parallel}(\infty) = 0 \qquad (2.19)$$

since a spatially localised mode is under consideration and the radial component of the perturbed magnetic field at the conducting wall must vanish.

3. MICROTEARING MODES IN A TWO ION SPECIES PLASMA

Assuming that a plasma contains a single ion species with $T_e = T_i$ and $Z = 1$ is not usually justified in a tokamak. In most discharges $Z_{eff} \neq 1$ and $T_i > T_e$ in discharges with neutral beam injection. The theory of the previous section may be extended to exclude the limiting assumptions. This is achieved by representing the different impurity ion species populating the tokamak plasma by a sole species of impurity ion.

The densities of the ionised filling gas, n_{ia}, and the impurity ions, n_{ib}, with atomic charges Z_a and Z_b respectively, are then related to Z_{eff} and n_e by

$$n_e = Z_a\, n_{ia} + Z_b\, n_{ib}$$
$$n_e\, Z_{eff} = n_{ia}\, Z_a^2 + n_{ib}\, Z_b^2 \qquad (3.1)$$

Substituting $n_{ia} = f_a\, n_e$ and $n_{ib} = f_b\, n_e$ in these equations allows the two constants f_a and f_b to be determined in terms of Z_a, Z_b and Z_{eff}.

From equation (2.12), the total perturbed charge density, Q_T, is the sum of the perturbation in charge density of each ion species :

$$Q_T = -(Z_a e)^2 n_{ia}/T_{i1}\, \{1 - \Gamma_0(b_1)(\omega+\omega_{*a})/\omega - \rho_1^2/2\, |\Gamma_0'(b_1)|\, (\omega+\omega_{*a})/\omega\, \delta^2/\delta x^2 \}\, \varphi$$
$$-(Z_b e)^2 n_{ib}/T_{i2}\, \{1 - \Gamma_0(b_2)(\omega+\omega_{*b})/\omega - \rho_2^2/2\, |\Gamma_0'(b_2)|\, (\omega+\omega_{*b})/\omega\, \delta^2/\delta x^2 \}\, \varphi$$
where $b_1 = k_y^2 \rho_1^2/2$ and $b_2 = k_y^2 \rho_2^2/2$. (3.2)

Assuming $T_i = T_{i1} = T_{i2}$ and letting $\tau = T_i/T_e$, then from equations (2.8) and (2.9) :

$$\omega_{*a} = (\tau/Z_a)\, \omega_{*e}$$
$$\omega_{*b} = (\tau/Z_b)\, \omega_{*e} \qquad (3.3)$$
$$\rho_2^2/2 = (M_2/M_1)\, (Z_a/Z_b)^2\, \rho_1^2 = L\, \rho_1^2/2 = L\, \rho_*^2$$

where M_2/M_1 is the ratio of the masses of the two ion species. Noting that :

$$Z_a^2\, n_{ia} e^2/T_i = \varepsilon_0\, (c^2/v_{A1}^2)\, /\rho_*^2 \qquad (3.4)$$

and letting $\kappa = (f_b/f_a)\, (Z_b/Z_a)^2$ allows Q_T to be written in the following form :

$$Q_T = \varepsilon_o (c^2/v_{A1}^2) / (\rho_*^2\omega) \qquad (3.5)$$

$$x \{ (\omega - \Gamma_o(b_1)(\omega+\tau\omega_{*e}/Z_a) - \rho_*^2 |\Gamma_o'(b_1)| (\omega+\tau\omega_{*e}/Z_a) \delta^2/\delta x^2)$$

$$+ \kappa(\omega - \Gamma_o(b_2)(\omega+\tau\omega_{*e}/Z_b) - L \rho_*^2 |\Gamma_o'(b_2)|(\omega+\tau\omega_{*e}/Z_b) \delta^2/\delta x^2) \} \varphi$$

Since $n_e e^2/T_e = \tau (n_e/n_{ia}) (n_{ia}e^2/T_i)$ then from equation (2.8) Q_e is given by :

$$Q_e = -k_{\parallel} \sigma_{\parallel e} E_{\parallel} /\omega + \varepsilon_o (\tau/(Z_a^2 f_a)) (c^2/v_{A1}^2) (1/\rho_*^2) (\omega_{*e}/\omega) \varphi \qquad (3.6)$$

Applying the quasi-neutrality condition and equation (2.15) with $X = x/\rho_i$ and $\phi = \varphi/v_{A1}$ then :

$$\{ |\Gamma_o'(b_1)| (W+\tau/Z_a) + \kappa (L |\Gamma_o'(b_2)| (W+\tau/Z_b)) \} \delta^2\phi/\delta X^2 \qquad (3.7)$$

$$= 2\{ \tau/(f_a Z_a^2) + W - \Gamma_o(b_1)(W+\tau/Z_a) + \kappa(W - \Gamma_o(b_2)(W+\tau/Z_b)) \} \phi - CK(WA_{\parallel} - K\phi)$$

The equation above and the Ampere's Law of equation (2.16) may also be solved by the invariant imbedding method. It will be assumed that $Z_a = 1$ (hydrogen) and $Z_b = 8$ (oxygen). Therefore $M_2/M_1 = 16$ and $M_1/m_e = 1836$.

4. PARALLEL ELECTRON CONDUCTIVITY

The derivation of the parallel electron conductivity, $\sigma_{\parallel e}$, is outlined in this section [5,11]. The collision operator, C_{ei} of the Fokker-Planck equation takes the following form when electron-ion collisions are considered [17] :

$$C_{ei} = \upsilon(v)/2 \; \delta/\delta\underline{v} \; . \; (\; v^2 \; \underline{I} - \underline{v} \; \underline{v} \;) \; . \; \delta/\delta\underline{v} \qquad (4.1)$$

where $\upsilon(v) = 3\sqrt{\pi}/4 \; (v_e/v)^3 \; / \tau_{ei}$

$$= 3.86 \times 10^{-12} \; n_i[m^{-3}] \; Z_i^2 \; \ln \Lambda \; (v_e/v)^3 \; / \; T_e[eV]^{3/2} \qquad (4.2)$$

τ_{ei} = the electron-ion collision time of Braginskii [18]

and $\ln \Lambda$ = the Coulomb logarithm

$$= 31.3 - 0.5 \ln (\; n_e[m^{-3}] \;) + 1.5 \ln (\; T_e[eV] \;) \qquad (4.3)$$

The Fokker-Planck equation for the electrons is :

$$(\; \delta/\delta t + \underline{v}.\delta/\delta\underline{x} + \underline{F}/m_e.\delta/\delta\underline{v} \;) \; f_e = C_{ei} \; f_e \qquad (4.4)$$

where f_e is the electron velocity distribution function and $\underline{F} = -e \; (\; \underline{E} + \underline{v} \times \underline{B} \;)$. A first order perturbation, f_{e1}, results from the perturbations in the electric and magnetic fields. Letting :

$$f_e = f_{eo} + f_{e1}$$

$$\underline{B} = \underline{B}_o + \underline{b} \qquad (4.5)$$

and retaining first order terms yields :

$$(\; \delta/\delta t + \underline{v}.\delta/\delta\underline{x} - C_{ei} \;) \; f_{e1} = (e/m_e) \; (\; \underline{E} + \underline{v} \times \underline{b} \;).\delta f_{eo}/\delta\underline{v} + \omega_{ce} \; \delta f_{e1}/\delta\alpha \qquad (4.6)$$

Cylindrical co-ordinates in velocity space are used :

$$\underline{v} = (\; v_r, \; \alpha, \; v_{\parallel} \;) \qquad (4.7)$$

The expression for the last term in equation (4.6) arises since Coulomb collisions result in pitch-angle scattering which produces perturbations in $v_{\parallel}$ and α only. In addition, the α dependence of f_{e1} is weak [11]. This term may be neglected when averaged over α, since it is small when compared to the other term on the right hand side of equation (4.6).

Assuming the perturbations of f_e are of the form :

$$f_{e1} = f_e(v_{\|}) \exp (-i\omega t + ik_y y + ik_{\|} z) \qquad (4.8)$$

then equation (4.6) is simplified to :

$$\{ i (\omega - k_{\|}v_{\|}) + \upsilon(v)/2 [\delta/\delta v_{\|} (v^2 - v_{\|}^2) \delta/\delta v_{\|}] \} f_{e1} \qquad (4.9)$$
$$= (e/m_e) (\underline{E} + \underline{v} \times \underline{b}).\delta f_{eo}/\delta \underline{v}$$

The electron energy, and hence the quantity v^2, remains approximately constant during the pitch angle scattering of the electrons from the ions. By taking $\xi = v_{\|}/v$ the above equation reduces to :

$$\{ i (\omega - k_{\|}v_{\|}) + \upsilon(v)/2 [\delta/\delta\xi (1-\xi^2) \delta/\delta\xi] \} f_{e1} \qquad (4.10)$$
$$= (e/m_e) (\underline{E} + \underline{v} \times \underline{b}).\delta f_{eo}/\delta \underline{v}$$

In the presence of density and temperature gradients then [11] :

$$f_{eo} = f_M (1 + P_z U_z/T_e + P_y U_y^n/T_e + P_y U_y^T/T_e (H - 3T_e/2)/T_e^2) \qquad (4.11)$$

where $f_M = n_e(x) \left(\dfrac{m_e}{2\pi T_e(x)} \right)^{3/2} \exp (-H/T_e(x))$

$$P_y = m_e v_y \qquad P_z = m_e v_{\|} - eA_{\|} \qquad H = m_e v^2/2$$
$$U_y^T = T_e/(eBL_T) \qquad U_y^n = T_e/(eBL_n) \qquad U_z = B/(\mu_o n_e e L_s) \qquad (4.12)$$
$$L_T = T_e/(\delta T_e/\delta x) \qquad L_n = n_e/(\delta n_e/\delta x)$$

Noting that :

$$(e/m_e) \delta/\delta \underline{v} = e (\underline{v} \delta/\delta H + \delta/\delta \underline{P})$$
$$(\underline{E} + \underline{v} \times \underline{b})_y = -ik_y (\varphi - v_{\|}A_{\|}) \qquad (4.13)$$

and recognising that the term in $\delta f_{eo}/\delta P_z$ may be neglected in the vicinity of the tearing layer [5,11] allows equation (4.10) to be further simplified :

$$\{ i (\omega - k_{\|}v_{\|}) + \upsilon(v)/2 [\delta/\delta\xi (1-\xi^2) \delta/\delta\xi] \} f_{e1}$$
$$= ev_{\|}E_{\|} \delta f_{eo}/\delta H - iek_y(\varphi - v_{\|}A_{\|}) \delta f_{eo}/\delta P_y \qquad (4.14)$$

The expansion of f_{e1} in a Legendre series :

$$f_{e1} = \Sigma b_n P_n(\xi) \qquad (4.15)$$

where the Legendre polynomials, $P_n(\xi)$, satisfy [19] :

$$\delta/\delta\xi (1-\xi^2)(\delta/\delta\xi P_n(\xi)) = -n (n-1) P_n(\xi) \qquad (4.16)$$

allows recurrence relations for the b_n to be obtained [20]. From :

$$j_{\parallel} = \int v_{\parallel} f_{e1} \, d^3\underline{v} = \sigma_{\parallel e} E_{\parallel} \tag{4.17}$$

an expression for $\sigma_{\parallel e}$ may then be found [5] :

$$\sigma_{\parallel e} = \frac{-8i}{3\sqrt{\pi}} \omega_{pe}^2 \varepsilon_o \int_0^{\infty} ds \; s^4 \exp(-s^2) \; \frac{(\omega - \omega_{*e}(1+\eta_e(s^2 - 3/2)))}{i\omega(i\omega - v(s))(1+\alpha_1) + k_{\parallel}^2 v_e^2 s^2/3} \tag{4.18}$$

where $s = v/v_e$ and $\eta_e = L_T/L_n$. The term, α_1, is given by a continuous fraction :

$$\alpha_n = \frac{(k_{\parallel}v)^2 (n+1)^2 (1+\alpha_{n+1})^{-1}}{(2n+1)(2n+3)(i\omega-(n+1)(n+2)v/2)(i\omega-n(n+1)v/2)} \tag{4.19}$$

Assuming a single ion species plasma, $Z = 1$ and $T_e = T_i$ then the expressions for C and α_n may be written in the following form :

$$C = \frac{8}{3\sqrt{\pi}} \frac{\omega_{pe}^2 \rho_i^2}{c^2} \int_0^{\infty} ds \;\; s^4 \exp(-s^2) \; \frac{(W - (1+\eta_e(s^2 - 3/2)))}{iW(iW - v_*/s^3)(1+\alpha_1) + U^2 s^2/3} \tag{4.20}$$

$$\alpha_n = \frac{(Us)^2 (n+1)^2 (1+\alpha_{n+1})^{-1}}{(2n+1)(2n+3)(iW-(n+1)(n+2)v_*/(2s^3))(i\omega-n(n+1)v_*/(2s^3))} \tag{4.21}$$

where $U = k_{\parallel}^2 v_e^2/\omega_{*e}^2 = 4 (M_i/m_e) (L_n/L_s)^2 X^2$. The value of v_* is found from equation (4.2) and the definition of ω_{*e} in equation (2.8). The term $\omega_{pe}^2 \rho_i^2/c^2$ may be simplified to $(\beta/2)(M_i/m_e)$. The solution of the coupled second order differential equations then require that β, L_n/L_s, η_e, $k_y\rho_i$, amd M_i/m_e be specified.

In a plasma containing two ion species, the collision operator on the right hand side of equation (4.4) must be summed over the two species of ions. The value v_* may then be found from equation (4.2) by replacing $n_i Z_i^2$ with $n_e Z_{eff}$. The expression for C must be altered as :

$$\frac{\omega_{pe}^2 \rho_1^2}{c^2} = \frac{M_1}{Z_a^2 m_e} \frac{n_e T_i}{B_o^2/(2\mu_o)} = \frac{M_1}{m_e} \frac{\tau \beta_e}{Z_a^2} \tag{4.22}$$

The expression for K must also be altered :

$$K = k_{\parallel} v_{A1} / \omega_{*e} = 2 (L_n / L_s) (\tau / (f_a \beta_e))^{1/2} X \qquad (4.23)$$

When $T_e = T_i$ and $Z_{eff} = 1$, then $\beta = 2\beta_e$, $\tau = 1$ and $f_a = 1$. The equations above are then consistent with equation (2.15).

5. SOLUTION OF DIFFERENTIAL EQUATIONS

The coupled second order differential equations are solved by the invariant imbedding method [16]. Details of the algorithm necessary for the coding of this problem are outlined in this section. A comprehensive description of the algorithm may be found in Ref. 16.

Consider the coupled second order differential equation in the form :

$$\begin{pmatrix} A_{\parallel}'' \\ \phi'' \end{pmatrix} = \begin{pmatrix} a_{11} & a_{12} \\ a_{21} & a_{22} \end{pmatrix} \begin{pmatrix} A_{\parallel} \\ \phi \end{pmatrix}$$

$$= \mathbf{A} \begin{pmatrix} A_{\parallel} \\ \phi \end{pmatrix} \tag{5.1}$$

The two linearly independent solutions of these equations may be represented by :

$$\begin{pmatrix} A_{\parallel 1} \\ \phi_1 \end{pmatrix} \quad \text{and} \quad \begin{pmatrix} A_{\parallel 2} \\ \phi_2 \end{pmatrix} \tag{5.2}$$

A matrix R is introduced with :

$$\mathbf{N} = \begin{pmatrix} A_{\parallel 1} & A_{\parallel 2} \\ \phi_1 & \phi_2 \end{pmatrix} = \begin{pmatrix} r_{11} & r_{12} \\ r_{21} & r_{22} \end{pmatrix} \begin{pmatrix} A_{\parallel 1}' & A_{\parallel 2}' \\ \phi_1' & \phi_2' \end{pmatrix} \tag{5.3}$$

$$= \mathbf{R}\,\mathbf{M}$$

and $$\mathbf{M}' = \begin{pmatrix} A_{\parallel 1}'' & A_{\parallel 2}'' \\ \phi_1'' & \phi_2'' \end{pmatrix} = \mathbf{A}\,\mathbf{N} \tag{5.4}$$

The two matrix equations above may be combined :

$$\mathbf{M} = \mathbf{R}'\,\mathbf{M} + \mathbf{R}\,\mathbf{A}\,\mathbf{R}\,\mathbf{M} \tag{5.5}$$

Assuming M to be non-singular yields a set of 4 first order differential equations in the complex components of R :

$$\mathbf{R}' = \mathbf{R}\,\mathbf{A}\,\mathbf{R} \tag{5.6}$$

As the matrix A is singular at the origin, the components of the matrix R grow in the vicinity of the origin. By introducing a matrix S which satisfies :

$$K = \begin{pmatrix} A_{II1}' & A_{II2}' \\ \phi_1 & \phi_2 \end{pmatrix} = \begin{pmatrix} s_{11} & s_{12} \\ s_{21} & s_{22} \end{pmatrix} \begin{pmatrix} A_{II1} & A_{II2} \\ \phi_1' & \phi_2' \end{pmatrix} \tag{5.7}$$

$$= S\ L$$

a set of 4 first order differential equations in the complex components of S when the matrix equation above is combined with equation (5.1) :

$$S' = -S \begin{pmatrix} 1 & 0 \\ 0 & a_{22} \end{pmatrix} - S \begin{pmatrix} 0 & 0 \\ a_{21} & 0 \end{pmatrix} + \begin{pmatrix} 0 & a_{12} \\ 0 & 0 \end{pmatrix} S + \begin{pmatrix} 1 & 0 \\ 0 & a_{22} \end{pmatrix} S \tag{5.8}$$

The initial conditions $A_{II}(\infty) = \phi(\infty) = 0$ are used at some finite value of X (typically X = 30). This requires that the initial values of the components of R are :

$$r_{11} = r_{12} = r_{21} = r_{22} = 0 \tag{5.9}$$

The first order differential equations are then solved over a finite extent in X until $| r_{11} | > 1$ (typically X = 25). At this point the relationship between the components of R and S are used to provide the initial values of the components of S :

$$s_{11} = 1/r_{12} \qquad s_{12} = -r_{12}/r_{11}$$

$$s_{21} = r_{21}/r_{22} \qquad s_{22} = r_{22} - r_{21}r_{12}/r_{11} \tag{5.10}$$

The first order differential equations in the components of S are then solved over the remaining extent in X. The solution of the differential equations are halted at $X = \xi = 10^{-6}$ as there exists a singularity at the origin.

Satisfying the boundary conditions of equation (2.17) at the origin is equivalent to the requirement that det S = 0 at $X = \xi$ [16]. The procedure to determine the eigenvalue, W, satisfying these boundary conditions begins with an initial guess, W_{1a}. The system of first order differential equations are solved using this eigenvalue. Then :

$$(\det S)_a = (S_{ra} , Sia) \tag{5.11}$$

is evaluated at $X = \xi$, where (x , y) represents the complex number x + iy.

Two further eigenvalues are tested :

$$W_{1b} = W_{1a} + (\delta W_r , 0)$$
$$W_{1c} = W_{1a} + (0 , \delta W_i) \qquad (5.12)$$

and typically $\delta W_r = 0.002$ and $\delta W_i = 0.001$ were used. The value of $(\det S)_b$ and $(\det S)_c$ are then calculated.

The change in the eigenvalue $(\Delta W_r, \Delta W_i)$ estimated to yield $\det S = 0$ is found from :

$$\begin{pmatrix} S_{ra} \\ S_{rb} \end{pmatrix} = \begin{pmatrix} \delta S_r/\delta W_r & \delta S_r/\delta W_i \\ \delta S_r/\delta W_r & \delta S_r/\delta W_r \end{pmatrix} \begin{pmatrix} \Delta W_r \\ \Delta W_i \end{pmatrix}$$
$$= D \begin{pmatrix} \Delta W_r \\ \Delta W_i \end{pmatrix} \qquad (5.13)$$

The components of the matrix D are derived from the 3 values of det S. The estimate of the new eigenvalue is then $W_{2a} = W_{1a} + (\Delta W_r , \Delta W_r)$. The iteration halts when $\det S < \xi$ is satisfied (typically $\xi = 10^{-4}$).

The eigenfunctions corresponding to the eigenvalue W are found by considering the differential equations for the components of $Q = M^{-1}$:

$$Q' = Q \; A \; R \qquad (5.14)$$

The initial values for the components of Q are chosen with the restriction that the vectors comprising M are linearly independent. Choosing :

$$Q = \begin{pmatrix} 1 & 0 \\ 0 & 1 \end{pmatrix} \qquad (5.15)$$

at $X = L$ and storing the components of Q at regular intervals while "shooting" the differential equations toward the origin allows M and N to be calculated in the interval where R is known. The linearly independent vectors, formed from the components of M, are therefore also known.

The differential equations for the components of $P = L^{-1}$ are considered in the interval where S is known :

$$P' = - P \begin{pmatrix} 1 & 0 \\ 0 & a_{22} \end{pmatrix} S + \begin{pmatrix} 0 & 0 \\ a_{21} & 0 \end{pmatrix} \tag{5.16}$$

The initial values of P are a function of the components of M and N :

$$L = \begin{pmatrix} A_{\parallel 1} & A_{\parallel 2} \\ \phi_1' & \phi_2' \end{pmatrix} = \begin{pmatrix} n_{11} & n_{12} \\ m_{21} & m_{22} \end{pmatrix} \tag{5.17}$$

The components of L and K are therefore the components of the linearly independent vectors. The solution is in terms of Q and P rather than their inverses M and L since the matrix components decrease when "shooting" towards the origin.

On the first shot towards the origin the values of the normalising coefficients c_1 and c_2 are determined from the components of K and L at $X = \xi$:

$$c_1 = -k_{22} / (k_{21} l_{12} - k_{22} l_{11})$$
$$c_2 = -k_{21} / (k_{21} l_{12} - k_{22} l_{11}) \tag{5.18}$$

The eigenfunction is then able to be constructed on the second shot towards the origin :

$$\begin{pmatrix} A_{\parallel} \\ \phi \end{pmatrix} = \begin{pmatrix} n_{11} & n_{12} \\ n_{21} & n_{22} \end{pmatrix} \begin{pmatrix} c_1 \\ c_2 \end{pmatrix} \quad \text{in the region where R is known}$$
$$= \begin{pmatrix} l_{11} & l_{12} \\ k_{21} & k_{22} \end{pmatrix} \begin{pmatrix} c_1 \\ c_2 \end{pmatrix} \quad \text{in the region where S is known} \tag{5.19}$$

6. NUMERICAL RESULTS

Confidence in the programming of the algorithm to determine the eigenvalue which satisifies the boundary conditions, is founded on a comparison of the obtained eigenvalue with those published in the literature.

Two references give eigenvalues for the microtearing mode using the set of parameters $\beta_e = 0.005$, $k_y \rho_i = 0.1$, $L_n/L_s = 0.05$, $\eta_e = 1$, $\tau = 1$, $Z = 1$ and $\upsilon_* = 10$. In Ref. 5 it is found that $W = 2.22 + i\ 0.063$, and in Ref. 8 it is found that $W = 2.215 + i\ 0.062$. The eigenvalue obtained by the author is $W = 2.220 + i\ 0.0623$. The eigenfunction corresponding to this eigenvalue is shown in Fig. 1. On a CRAY XMP-2, approximately 5 seconds of CPU time is required to test an eigenvalue and evaluate det S.

It is also of interest to compare the eigenvalues obtained when either a one or two ion species plasma is assumed. Taking $Z_a = 3$, $Z_{eff} = 3$ and the other parameters as above, then for a one ion species plasma an eigenvalue of $W = 2.183 - i\ 0.234$ is obtained. Taking $Z_{eff} = 3$ and $Z_a = 1$ then for a two ion species plasma an eigenvalue $W = 2.213 + i\ .0593$ is obtained. It is evident that the assumption of a single ion species leads to the instability of the mode being underestimated. For a deuterium plasma ($Z_{eff} = 3$, $Z_a = 1$, $M_2/M_1 = 8$ and $M_1/m_e = 3672$.) an eigenvalue of $W = 2.177 + i\ .0619$ is obtained. The stability of the microtearing mode is then not very sensitive to this change from hydrogen to deuterium.

An investigation of the stability of microtearing modes in ASDEX require that the radial profiles of n_e, T_e, T_i, and q(r) are available, so that the set of parameters β_e, L_n/L_T, τ, $k_y\rho_i$, η_e, υ_*, and Z_{eff} may be specified. These radial profiles were obtained from the BALDUR code [21]. Experimental measurements of of n_e, T_e and T_i show that the radial profiles predicted by the BALDUR transport

code are within experimental error. Away from the separatrix, the radial profiles and T_i may be parameterised in terms of the normalised radius $x = r/a$:

$$f(x) = \alpha_4 + \alpha_1 \, (\, 1 - x^{\alpha_3} \,)^{\alpha_2} \qquad (6.1)$$

The radial profile of q(r) may be parameterised in the form :

$$f(x) = \alpha_1 \, (\, 1 + \alpha_4 \, x^{\alpha_3} \,)^{\alpha_2} \qquad (6.2)$$

It has been noted that mode stability is strongly dependent on the radial position of the mode rational surface and the peakedness of the radial profiles [5]. In Fig. 2 the radial profiles of n_e, T_e, T_i, and q(r) in an ohmic discharge are displayed. The values of α_1, α_2, α_3 and α_4, that yield a least squares fit to the radial profiles in the ohmic, L and H discharges considered, are listed in Tables 1 and 2. In Figs. 3, 4, 5 and 6 the real and imaginary part of the eigenvalue, ω, for modes with $m = 5, 8, 10$ and 15 in these discharges are plotted. For ohmic discharges, unstable modes are positioned towards the plasma centre. In contrast, unstable modes are located closer to the plasma boundary in L and H discharges.

The variation in these calculated eigenvalues with respect to changes in the starting point of the numerical solution of the differential equations and the number of terms retained in the continuous fraction was tested. The eigenvalue was changed by less than 1% when the starting point was altered from $X = 30$ to $X = 60$. The eigenvalue was changed by less than 1% when the number of terms retained in the continuous fraction was varied from 8 to 12.

7. DISCUSSION

Recent experimental observations of turbulent magnetic fluctuations on Doublet III, TFTR, and JET [22-24], indicate that modes with m ≈ 10 may be responsible for the observed broadband spectrum of magnetic fluctuations.

Qualitatively, it would be expected that a given unstable mode is responsible for a particular frequency component of the turbulent spectrum. This simplistic view is obscured to some extent by the non-linear coupling of a finite number of unstable modes [25], which gives rise to a broadband spectrum rather than a spectrum consisting of a number of delta functions. It is difficult to quantatively apply linear microtearing mode theory to an experiment. Predictions of saturated amplitudes and the generation of a broadband spectrum may only be described by non-linear theories [26,27].

The capacity of the magnetic probe system installed on ASDEX to scan 8 cm in the radial direction in 150 ms, provides the opportunity to obtain an estimate of the poloidal mode number, m. Away from the mode rational surface, the amplitude of the mode decays as $r^{-(m+1)}$ in cylindrical geometry. Because of the strong radial dependence on m, such measurements are strongly weighted to the lowest unstable m number present.

Previously, the m number has been inferred from the radial decay of the magnetic fluctuation amplitude as measured by a number of probes located at different poloidal angles around the plasma and at different radii from the plasma [22]. It is not clear that these measurements would be in agreement with those made by a radially scanned probe, since the effects of toroidal geometry should influence the former measurements to a greater extent.

A correlation between the predicted unstable mode numbers and experimental measurements is not straightforward. However, recent experiments providing estimates of m could be improved by obtaining radial decay

measurements as a function of frequency. It could be expected that the higher frequency components would be dominated by those modes with a larger m number. The employment of narrow bandpass filters (or a "frequency comb" [24,28]) would allow these measurements to be obtained in a single discharge.

The interpretation of an increase or decrease in the amplitude of broadband magnetic fluctuations during L and H discharges must be interpreted with caution, since the amplitude observed is strongly dependent on the radial position of the instability. A comparison of the location of unstable modes in Fig. 4 and Fig. 6 shows that the zone of instability moves toward the plasma edge. An increase in the amplitude of magnetic fluctuations may either be due to a change in the radial position of unstable modes or an increase in the saturation level.

The change in the real frequency of the modes upon transition from an O to an L discharge, as shown in Figs. 3 and 4, suggests that a broader frequency band of magnetic fluctuations should be observed.

8. CONCLUSIONS

The linear stability of microtearing modes in typical ASDEX discharges have been calculated. In the case of Ohmic discharges it was found that unstable modes are predicted to be located towards the centre of the plasma. For L and H discharges the zone of instability shifts towards the plasma edge. The interpretation of an increase or decrease in the amplitude of broadband magnetic fluctuations during L and H discharges must be interpreted with caution, since the amplitude observed is strongly dependent on the radial position of the instability.

Although a comparison of theory and experiment is not straightforward, the capability of the magnetic probe system on ASDEX to determine the poloidal mode number from measurements of the radial decay in amplitude of the magnetic fluctuations at one poloidal location means that such measurements could be of value. An increase in the experimental database concerning broadband magnetic fluctuations in tokamaks is necessary for deciding whether the destruction of magnetic surfaces is responsible for anomalous electron transport.

9. REFERENCES

[1] P.C. Liewer,
Nucl. Fusion, 25, 543, 1985.

[2] A.B. Mikhailovskii,
Reviews of Plasma Physics (M.A.Leontovich, Ed.),
Vol. 3., 159, 1967.

[3] V.V. Parail and O.P. Pogutse,
Plasma Physics and Controlled Nuclear Fusion,
Proceedings of 8th International Conference, (Brussels),
Vol. 1, 67, 1981.

[4] D.A. D'Ippolito, Y.C. Lee, and J.F. Drake,
Phys. Fluids, 23, 771, 1980.

[5] N.T. Gladd, J.F. Drake, C.L. Chang and C.S. Liu,
Phys. Fluids, 23, 1182, 1980.

[6] M. Rosenberg, R.R. Dominguez, W. Pfeiffer and R.E. Waltz,
Phys. Fluids, 23, 2022, 1980.

[7] J.F. Drake, T.M. Antonsen, A.B. Hassam, and N.T. Gladd,
Phys. Fluids, 26, 2509, 1983.

[8] R. Farengo, Y.C. Lee and P.N. Guzdar,
Phys. Fluids, 26, 3515, 1983.

[9] Y.C. Lee, J.Q. Dong, P.N. Guzdar and C.S. Liu,
Phys. Fluids, 30, 1331, 1987.

[10] K.T. Tsang, J.C. Whitson and J. Smith,
Phys. Fluids, 22, 1689, 1979.

[11] J.F. Drake and Y.C. Lee,
Phys. Fluids, 20, 1347, 1977.

[12] H.P. Furth, J. Killeen and M.N. Rosenbluth,
Phys. Fluids, 6, 459, 1963.

[13] H.P. Furth, P.H. Rutherford, and H. Selberg,
Phys. Fluids, 16, 1054, 1973.

[14] R.D. Hazeltine, D. Dobrott, and T.S. Wang,
Phys. Fluids, 18, 1778, 1975.

[15] M. Abramowitz and I.A. Stegun,
"Handbook of Mathematical Functions",
p. 374, (U.S. Dept. of Commerce, 1964).

[16] J. Smith and J.C. Whitson,
J. Comput. Phys., 33, 102, 1979.

[17] S.I. Braginskii,
"Reviews of Plasma Physics", Vol. 1, p. 239.

[18] S.I. Braginskii,
"Reviews of Plasma Physics", Vol. 1, p. 215.

[19] M. Abramowitz and I.A. Stegun,
"Handbook of Mathematical Functions", p. 332.

[20] R.A. Koch and W. Horton Jr.,
Phys. Fluids, 18, 861, 1975.

[21] G. Becker, private communication.

[22] N. Ohyabu et al.,

Phys. Rev. Lett., 58, 120, 1987.

[23] M. Malacarne et al.,

JET Report, JET-P(87) 22.

[24] K. McGuire et al.,

PPPL Report, PPPL-2435, 1987.

[25] J.M. Wersinger, J.M. Finn and E. Ott,

Phys. Fluids, 23, 1142, 1980.

[26] R.R. Dominguez, M. Rosenberg and C.S. Chang,

Phys. Fluids, 24, 472, 1981.

[27] G.G. Craddock,

"Theoretical microtearing turbulence and related computational studies of constrained turbulent relaxation",

University of Texas, Institute of Fusion Studies, IFSR 295, 1987.

[28] C. Hollenstein et al.,

CRPP Report, LRP 306/86.

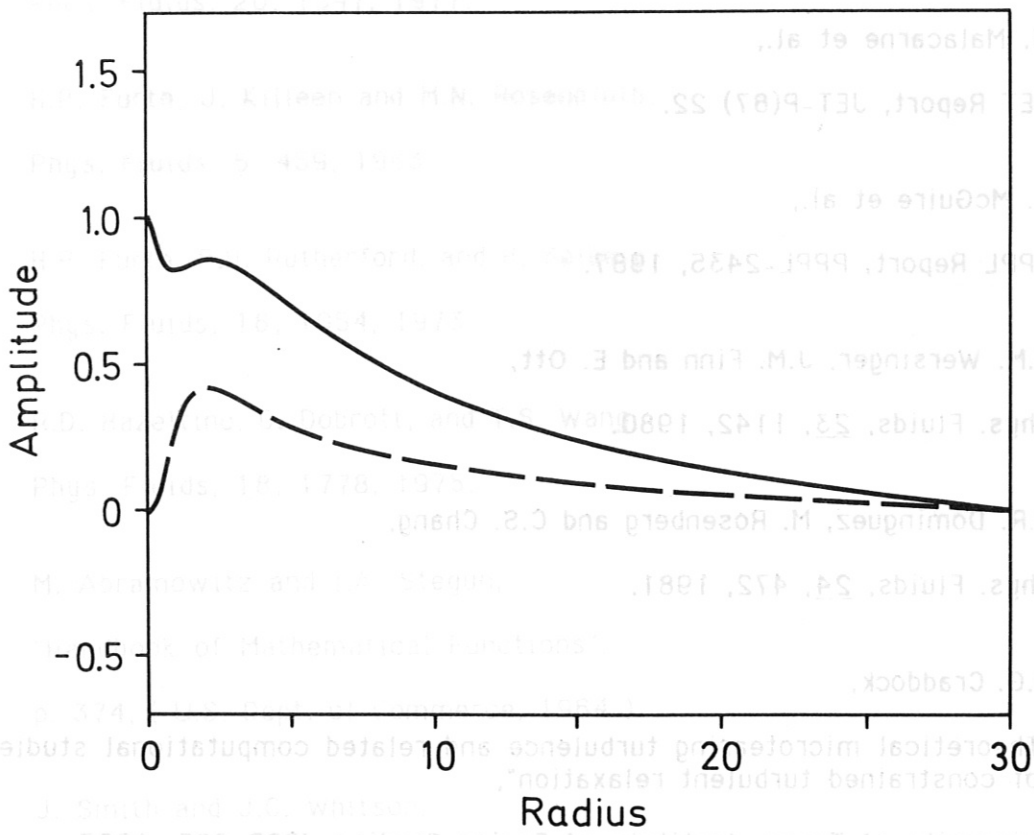

Fig. 1. The eigenfunction for $A_{\parallel}$ plotted versus radius $X = x/\rho_i$ for $\beta_e = 0.005$, $k_y\rho_i = 0.1$, $L_n/L_s = 0.05$, $\eta_e = 1$, $\tau = 1$, $Z_{eff} = 1$ and $\upsilon_* = 10$.

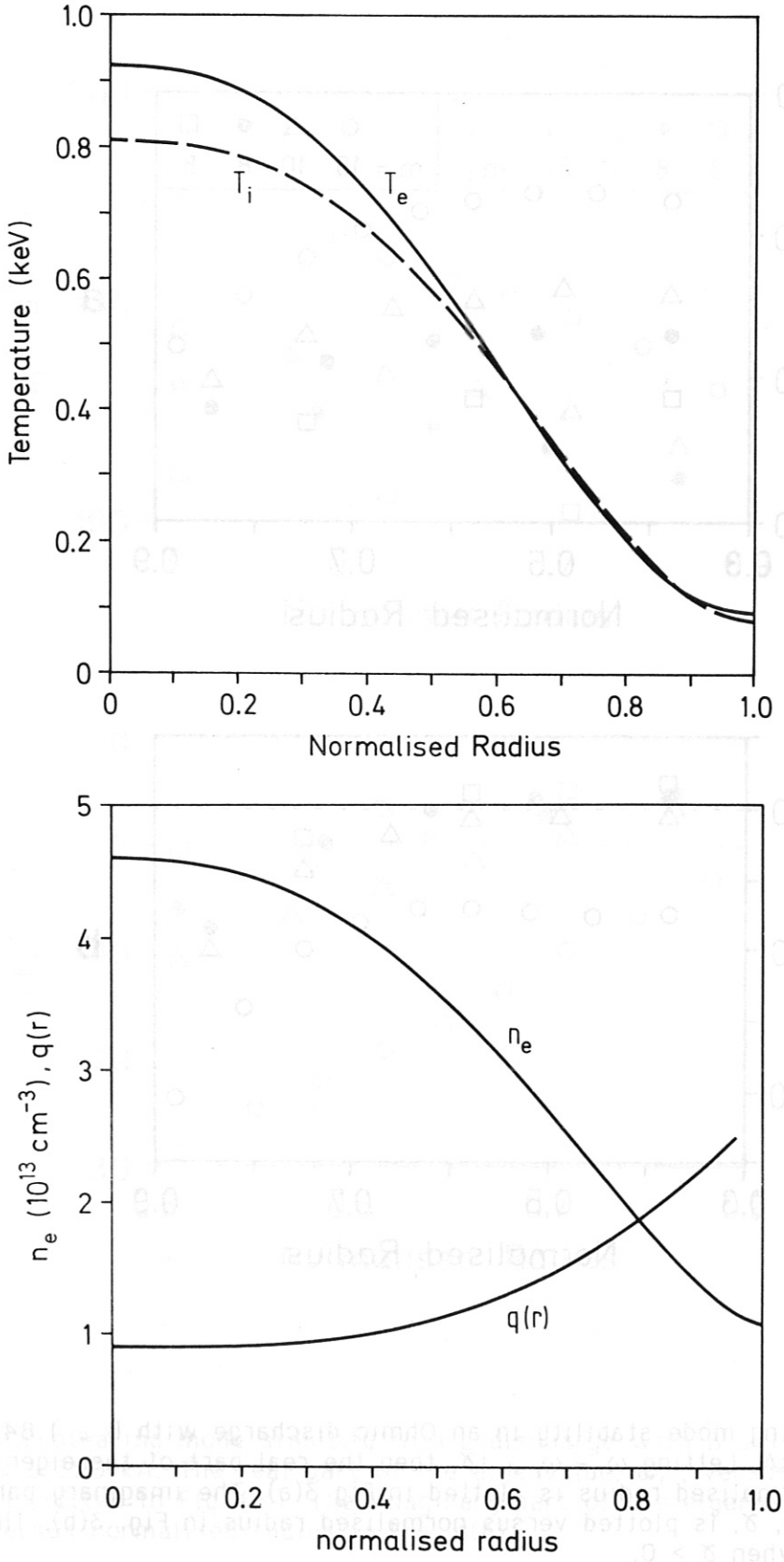

Fig. 2. The radial profiles of n_e, T_e, T_i and q for an Ohmic discharge (No. 18041).

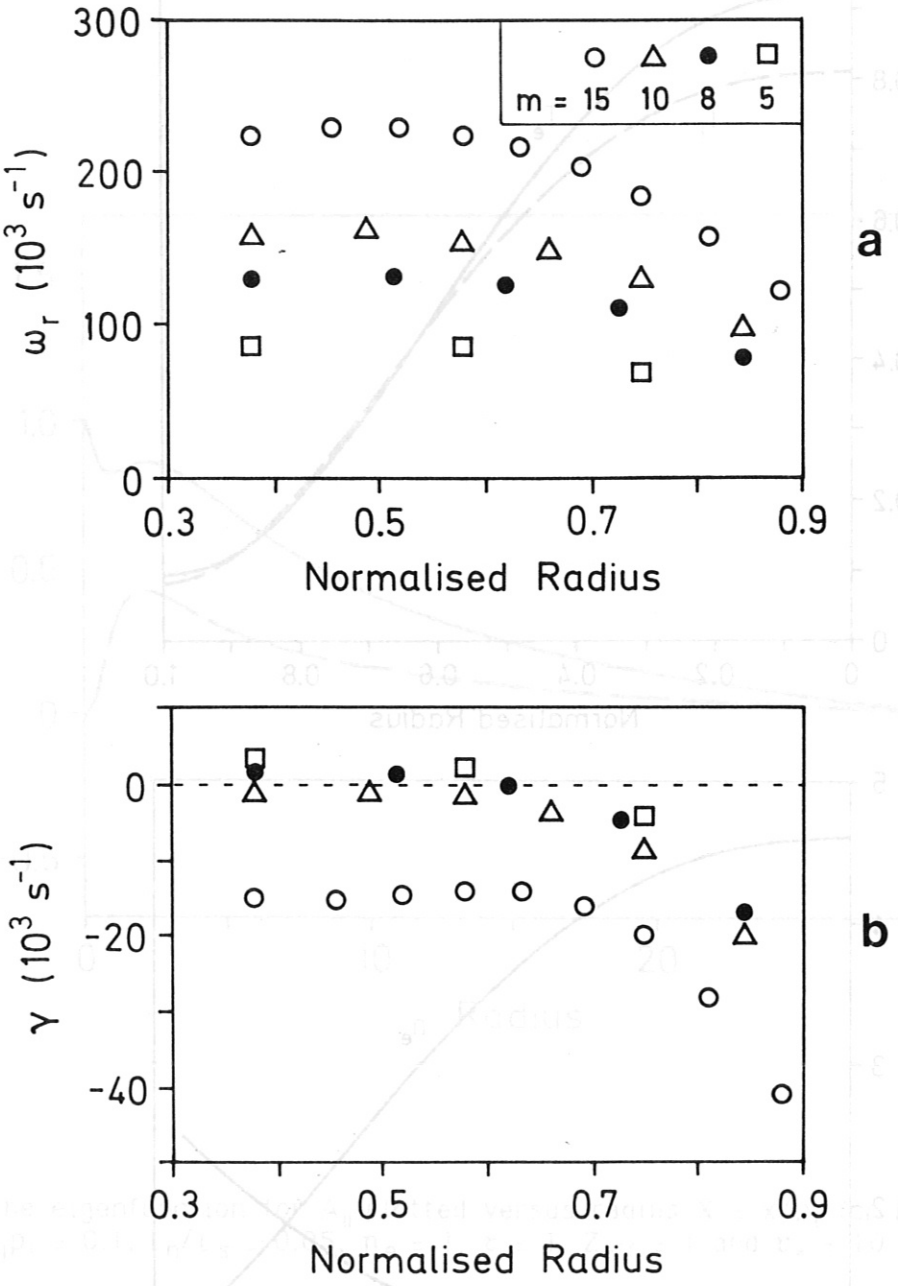

Fig. 3. Microtearing mode stability in an Ohmic discharge with B = 1.846 T and I_p = 320 kA. Letting $\omega = \omega_r + i\gamma$, then the real part of the eigenvalue, ω_r, versus normalised radius is plotted in Fig 3(a). The imaginary part of the eigenvalue, γ, is plotted versus normalised radius in Fig. 3(b). The mode is unstable when $\gamma > 0$.

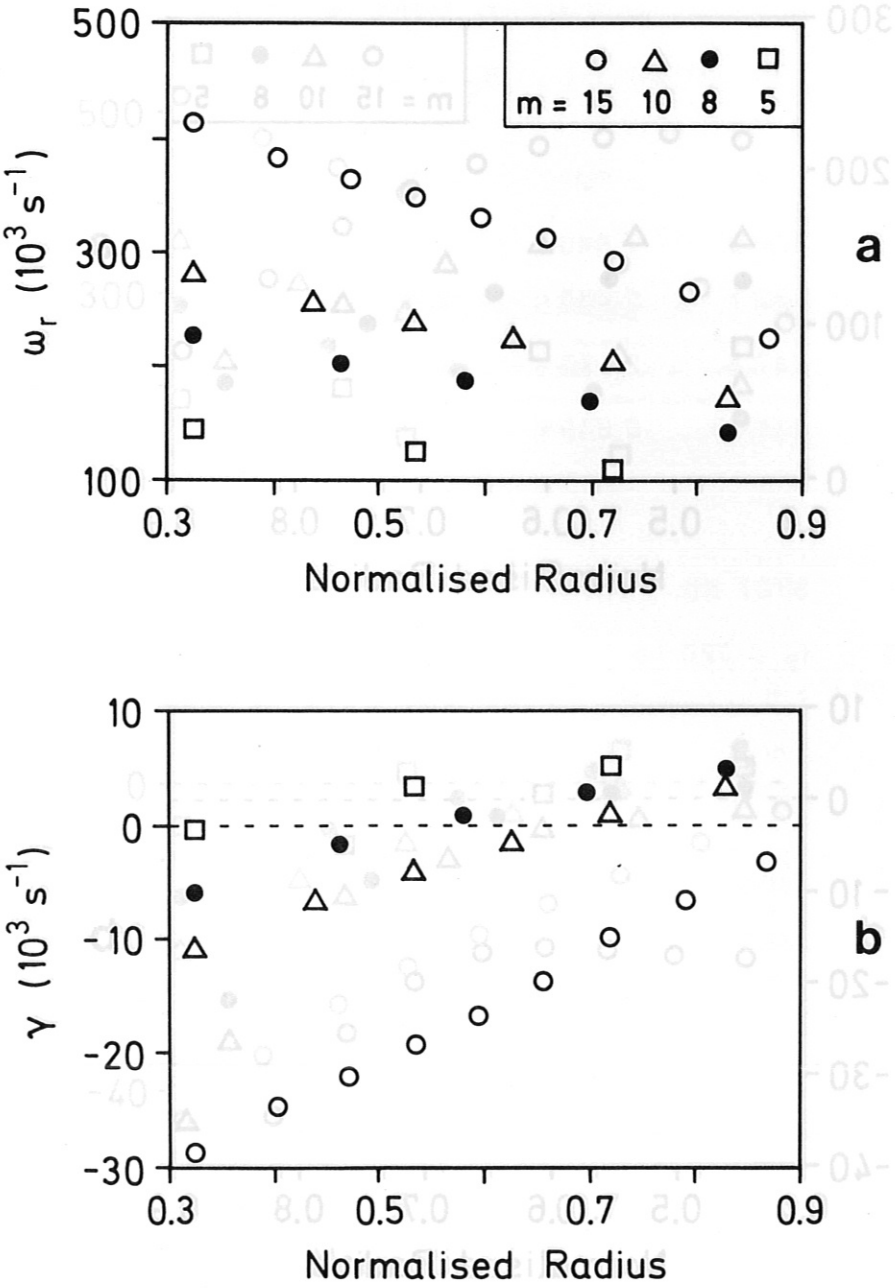

Fig. 4. Microtearing mode stability in a L discharge with B = 1.846 T and I_p = 320 kA. The real part of the eigenvalue, ω_r , versus normalised radius is plotted in Fig 4(a). The imaginary part of the eigenvalue, γ, is plotted versus normalised radius in Fig. 4(b).

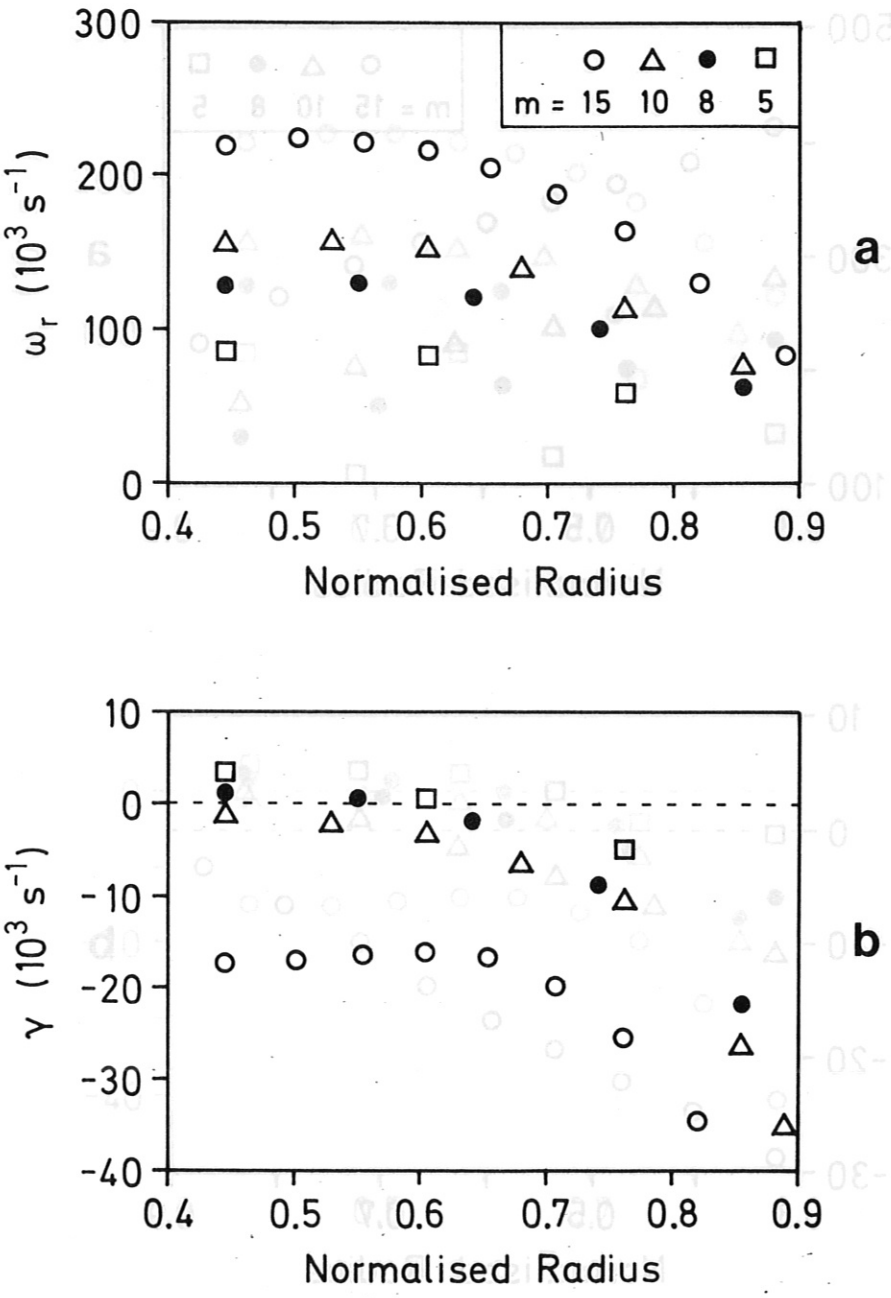

Fig. 5. Microtearing mode stability in an Ohmic discharge with B = 2.154 T and I_p = 380 kA. The real part of the eigenvalue, ω_r, versus normalised radius is plotted in Fig 5(a). The imaginary part of the eigenvalue, γ, is plotted versus normalised radius in Fig. 5(b).

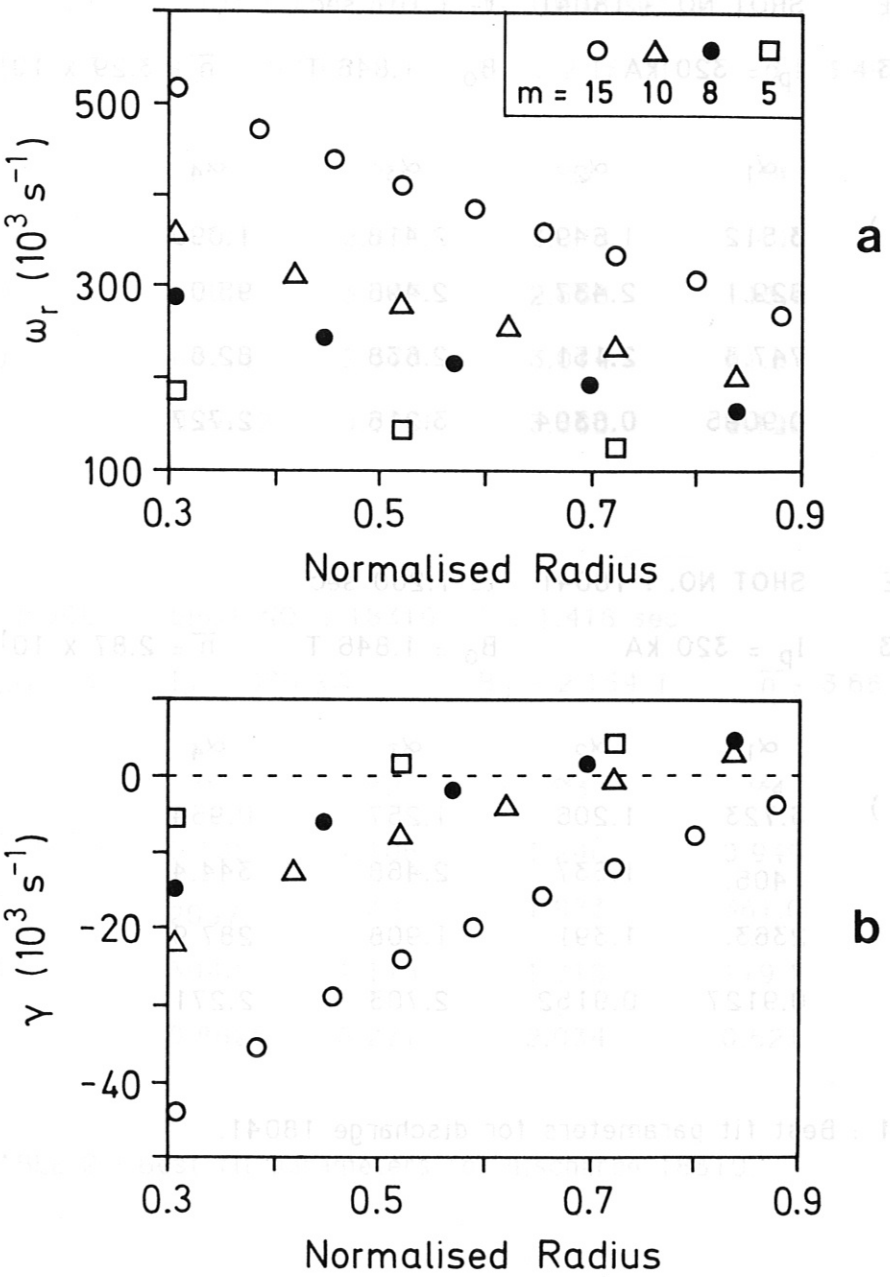

Fig. 6. Microtearing mode stability in a H discharge with B = 2.154 T and I_p = 380 kA. The real part of the eigenvalue, ω_r, versus normalised radius is plotted in Fig 6(a). The imaginary part of the eigenvalue, γ, is plotted versus normalised radius in Fig. 6(b).

O-MODE SHOT NO. : 18041 t= 1.101 sec

Z_{eff} = 3 I_p = 320 kA B_o = 1.846 T $\overline{n}$ = 3.29 x 10^{19}

	α_1	α_2	α_3	α_4
n_e (10^{19} m^{-3})	3.512	1.649	2.418	1.090
T_e (eV)	829.1	2.437	2.496	95.0
T_i (eV)	747.3	2.151	2.638	82.8
q(r)	0.9095	0.8304	3.216	2.727

L-MODE SHOT NO. : 18041 t= 1.200 sec

Z_{eff} = 3 I_p = 320 kA B_o = 1.846 T $\overline{n}$ = 2.87 x 10^{19}

	α_1	α_2	α_3	α_4
n_e (10^{19} m^{-3})	3.723	1.206	1.257	0.954
T_e (eV)	1405.	1.637	2.468	344.4
T_i (eV)	2363.	1.391	1.908	287.9
q(r)	0.9127	0.9152	2.703	2.271

TABLE 1 : Best fit parameters for discharge 18041.

O-MODE SHOT NO. : 18310 t= 1.097 sec

Z_{eff} = 3 I_p = 380 kA B_o = 2.154 T $\overline{n}$ = 3.49 x 10^{19}

	α_1	α_2	α_3	α_4
n_e (10^{19} m^{-3})	3.278	2.235	3.078	1.400
T_e (eV)	920.8	3.047	2.668	113.9
T_i (eV)	697.2	2.378	3.014	81.8
q(r)	0.8632	0.6206	3.660	5.126

H-MODE SHOT NO. : 18310 t = 1.418 sec

Z_{eff} = 3 I_p = 380 kA B_o = 2.154 T $\overline{n}$ = 3.68 x 10^{19}

	α_1	α_2	α_3	α_4
n_e (10^{19} m^{-3})	5.132	1.106	1.240	0.949
T_e (eV)	2097.	1.399	1.973	361.0
T_i (eV)	3940	1.173	1.716	119.1
q(r)	0.8825	2.277	2.034	0.621

TABLE 2 : Best fit parameters for discharge 18310.

11. ACKNOWLEDGEMENTS

The author is indebted to a number of people who assisted in the preparation of this report. Dr. S. Kaesdorf and Dr. U. Stroth were always available to discuss the various problems that arose in the time consuming task of writing the computer program. Special thanks to Dr. U. Stroth for the driving lessons on the CRAY and the donation of a plotting subroutine. The first draft of this report was read by Dr. K. Grassie and his invaluable comments brought many clarifications to this report. Dr. G. Becker willingly spent a large amount of time discussing various aspects of transport theory and the BALDUR code.

The patient typing of the first draft of this report by C. Weller and the professional drawing of the diagrams by E. Volkenandt were also very much appreciated.